Available online at www.sciencedirect.com
ScienceDirect
Journal of Computational Physics 225 (2007) 342–362
JOURNAL OF COMPUTATIONAL PHYSICS
www.elsevier.com/locate/jcp

An upwinding boundary condition capturing method for Maxwell's equations in media with material interfaces

Changfeng Xue [a,b], Shaozhong Deng [c,*]

[a] Department of Fundamental Sciences, Yancheng Institute of Technology, Yancheng, Jiangsu 224003, PR China
[b] State Key Laboratory of Turbulence and Complex Systems, Peking University, Beijing 100871, PR China
[c] Department of Mathematics and Statistics, University of North Carolina at Charlotte, Charlotte, NC 28223, United States

Received 23 July 2006; received in revised form 5 November 2006; accepted 2 December 2006
Available online 19 January 2007

Abstract

By using ghost points on either side of the interfaces, a global second-order accurate upwinding boundary condition capturing method for time-domain Maxwell's equations in media with material interfaces is proposed. The equations are discretized on a uniform Cartesian grid and the interfaces are allowed to intersect the grid in an arbitrary fashion. The method is then obtained by combining central finite difference schemes with applicable nodes being replaced by the ghost points and upwinding technique with jump conditions across the interfaces being captured in a manner that the upwind property is always satisfied. The resulting discretization has the desirable property that the allowed time step size is independent of the locations and the shapes of the interfaces. Numerical examples are then given to demonstrate the second-order accuracy as well as the stability of the method, where it is used to study wave equations with various types of material interfaces, including electromagnetic scattering of a plane incident wave by a dielectric circular cylinder.

AMS: 65M06; 78A45

Keywords: Finite-difference time-domain method; Ghost fluid method; Maxwell's equations

1. Introduction

The finite-difference time-domain (FDTD) methods, which were first introduced by Yee in 1966 [1] and later developed by Taflove and others [2], have been used extensively as useful modeling tools in computational electromagnetics and have been applied to a broad range of application problems. In particular, the most widely-used staggered Yee scheme [1] has been demonstrated to be robust, efficient, and simple to implement. However, when used to model objects with curved boundaries or to solve Maxwell's equations in media with irregular material interfaces, locally conforming meshes to the curved boundaries or the irregular material interfaces are required. Otherwise, the second-order Yee scheme may reduce to at best first-order accuracy and allow the possibility of localized non-convergent behavior [3,4]. Furthermore, when used to solve

* Corresponding author. Tel.: +1 704 687 6657; fax: +1 704 687 6415.
E-mail address: shaodeng@email.uncc.edu (S. Deng).

0021-9991/$ - see front matter
doi:10.1016/j.jcp.2006.12.001

Maxwell's equations with discontinuous coefficients, the Yee scheme might not be able to capture the possible discontinuity of the solution across the interfaces.

A number of second-order finite difference methods have been proposed in the past for modeling time-domain Maxwell's equations in inhomogeneous media with irregular material interfaces. The usual and straightforward approach is to introduce appropriate local modifications into the Yee scheme but still keep the staggered grid [4–6]. It should also be pointed out that there are some recent studies of high-order embedded boundary FDTD schemes for time-domain Maxwell's equations with material interfaces [7], including the non-dissipative staggered fourth-order explicit method and the staggered fourth-order compact implicit method by Yefet et al. [8,9], and the staggered fourth-order explicit method and the orthogonal curvilinear staggered-grid fourth-order explicit method by Xie et al. [10,11]. Subtle interface techniques with one-sided difference approximations and extrapolations are employed in these methods. Also, high-order FDTD methods via hierarchical implicit derivative matching are presented in [12]. The significant accomplishment of these high-order schemes is that the physical jump conditions at the material interfaces are correctly enforced up to high-order, so that high-order convergence is uniformly assured over the entire domain. The implementation of these high-order FDTD methods for Maxwell's equations in inhomogeneous media with complex material interfaces, however, has not been addressed with satisfactory results and therefore remains a great challenge.

Previous numerical methods making use of Cartesian grids for the approximation of hyperbolic equations could also be found in [13–16], among which is the fully second-order upwinding embedded boundary method (UEBM) [13]. This method makes use of a simple Cartesian grid and basically a central finite difference scheme for grid points away from the interfaces. To enforce the physically correct jump conditions across the interfaces, however, appropriate local modifications of the finite difference scheme close to the interfaces are developed with the use of one-sided difference approximations and extrapolations. In addition, solutions at both sides of the interfaces are also calculated and reconciled in order to observe both the upwind property and the interface jump condition.

The ghost fluid method (GFM) was originally designed to properly treat contact discontinuities in the inviscid Euler equations in [17], and since then it has been generalized to handle irregular boundaries in a variety of problems [18–30]. For examples, with the use of the so-called ghost cells (based on the GFM), Gibou et al. proposed in [22] a second-order accurate finite difference method for Poisson equations, and most recently in [23] a fourth-order accurate finite difference method for the Laplace and heat equations, on irregular domains with Dirichlet boundary conditions being imposed on the irregular interfaces. Similarly, by using ghost points on either side of the interfaces, Kreiss et al. proposed several second-order embedded boundary methods for second-order wave equations with Dirichlet boundary condition [27,28], Neumann boundary condition [29], and jump conditions [30] on the irregular interfaces, respectively.

In this paper, we shall combine the GFM with the UEBM to develop a new second-order accurate finite difference method for time-domain Maxwell's equations in media with material interfaces. First, the equations are discretized on a uniform Cartesian grid and the interfaces are allowed to intersect the grid in an arbitrary fashion. Then, like in the GFM [23], ghost points are introduced in the neighborhood of the interfaces, and used in the discretization of the spatial derivatives in the finite difference stencil. To capture the boundary conditions across the interfaces, like in the UEBM [13], the solutions at both sides of the interfaces are also calculated by one-sided extrapolations of the solution in the corresponding side of the interfaces. Since in hyperbolic systems, the upwind characteristic information should be unaffected by the material interfaces, the two interface solutions are so constructed that both the interface jump condition and the upwind property are observed. One- and two-dimensional numerical examples are presented at last to verify the global second-order accuracy as well as the stability of the method.

2. One-dimensional scalar wave equations

To demonstrate the basic idea of the upwinding boundary condition capturing method, we begin by considering the one-dimensional scalar wave equation

$$\frac{\partial u}{\partial t} + c\frac{\partial u}{\partial x} = 0, \quad x \in \Omega = [a, b], \tag{1}$$

where the wave speed c is assumed to be positive and discontinuous at $x_d \in (a,b)$, i.e.,

$$c = \begin{cases} c^- > 0, & x < x_d, \\ c^+ > 0, & x > x_d. \end{cases}$$

Consequently, the solution $u(x,t)$ is in general discontinuous at the interface x_d, and is assumed to satisfy the given interface jump condition

$$r^+ u(x_d^+, t) - r^- u(x_d^-, t) = g(t), \tag{2}$$

where $u(x_d^-, t)$ and $u(x_d^+, t)$ represent the two one-sided limits of the solution as x approaches the interface x_d, henceforth called the interface solutions.

To solve Eq. (1) by a finite difference method, the spatial computational domain $[a,b]$ is discretized into cells of size Δx to form a uniform Cartesian grid $\{x_i = a + i\Delta x,\ 0 \leqslant i \leqslant N,\ \Delta x = (b-a)/N\}$. Let u_i^n denote the numerical approximation of the solution $u(x_i, t_n)$, and also let $u^{-,n}$ and $u^{+,n}$ denote the numerical approximation of the interface solutions $u(x_d^-, t_n)$ and $u(x_d^+, t_n)$, respectively.

We shall construct a uniformly second-order finite difference method to solve Eq. (1) based on the Lax–Wendroff approach

$$u^{n+1} \doteq u^n + \Delta t u_t^n + \frac{(\Delta t)^2}{2} u_{tt}^n = u^n - c\Delta t u_x^n + \frac{c^2 (\Delta t)^2}{2} u_{xx}^n. \tag{3}$$

For each unknown u_i^{n+1}, the above Lax–Wendroff scheme is employed with the spatial derivatives being approximated by appropriate second-order central finite differences

$$u_x^n|_{x=x_i} \approx \frac{u_{i+1}^n - u_{i-1}^n}{2\Delta x}, \tag{4}$$

$$u_{xx}^n|_{x=x_i} \approx \frac{u_{i+1}^n - 2u_i^n + u_{i-1}^n}{(\Delta x)^2}. \tag{5}$$

However, the discretization (4) or (5) is valid only if all the nodes in the stencil belong to the same side of the interface, and needs to be modified otherwise. For example, suppose that the discontinuity lies between the nodes x_j and x_{j+1}, and $x_d = x_j + \theta\Delta x$ (see Fig. 1), where $0 \leqslant \theta < 1$ is called the cell fraction, and we seek to approximate u_x and u_{xx} at the grid point x_j in order to solve for u_j^{n+1}. Since the solution might not be smooth or even continuous across the interface, we need a valid value for u_{j+1}^n that can emulate the behavior of the solution defined to the left of the interface. As discussed in [23], this can be achieved by introducing a ghost cell around the discontinuity, or in another word, a ghost value $u_{j+1}^{n,\mathrm{G}}$ at x_{j+1} defined by extrapolation of the solution to the left side of the interface. Then, the spatial discretization (4) or (5) for the irregular grid point x_j can be rewritten as

$$u_x^n|_{x=x_j} \approx \frac{u_{j+1}^{n,\mathrm{G}} - u_{j-1}^n}{2\Delta x}, \tag{6}$$

$$u_{xx}^n|_{x=x_j} \approx \frac{u_{j+1}^{n,\mathrm{G}} - 2u_j^n + u_{j-1}^n}{(\Delta x)^2}. \tag{7}$$

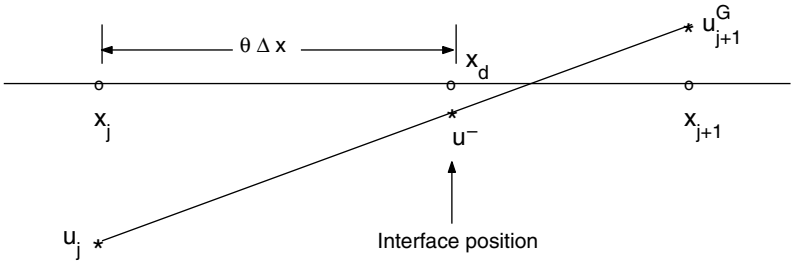

Fig. 1. Illustration of the definition of ghost values.

More precisely, we construct a linear extrapolant $L(x)$ of $u(x)$ to the left of the interface, such that $L(x_j) = u_j$ and $L(x_d) = u^-$. Then the ghost value at the node x_{j+1} is defined as $u^G_{j+1} = L(x_{j+1})$, and we have

$$u^G_{j+1} = L(x_{j+1}) = \frac{\theta - 1}{\theta} u_j + \frac{1}{\theta} u^-. \tag{8}$$

Considering that the cell fraction θ could be very small or even zero for an arbitrary grid, in practice when it is too small, we instead construct the linear extrapolant $L(x)$ such that $L(x_{j-1}) = u_{j-1}$ and $L(x_d) = u^-$. Note that in this case, we still use u^- rather than u_j in the extrapolation to take into account the boundary condition, and it is for this reason that, in addition to the solution at all grid points, at each time step we need to keep track of the solution at both sides of the interface as well. Accordingly, the ghost value at the node x_{j+1} is defined as $u^G_{j+1} = L(x_{j+1})$, and we have

$$u^G_{j+1} = L(x_{j+1}) = \frac{\theta - 1}{1 + \theta} u_{j-1} + \frac{2}{1 + \theta} u^-. \tag{9}$$

Similarly, to approximate u_x and u_{xx} at x_{j+1} when we solve for u^{n+1}_{j+1}, we would require a ghost value at the node x_j, denoted by $u^{n,G}_j$, which can emulate the behavior of the solution defined to the right of the interface as if no interface is present. Accordingly, the numerical discretization (4) or (5) of the spatial derivatives at x_{j+1} in terms of the ghost value would be

$$u^n_x|_{x=x_{j+1}} \approx \frac{u^n_{j+2} - u^{n,G}_j}{2\Delta x}, \tag{10}$$

$$u^n_{xx}|_{x=x_{j+1}} \approx \frac{u^n_{j+2} - 2u^n_{j+1} + u^{n,G}_j}{(\Delta x)^2}. \tag{11}$$

Here, the ghost value u^G_j could be obtained by a linear extrapolant $R(x)$ of $u(x)$ to the right of the interface, such that $R(x_{j+1}) = u_{j+1}$ and $R(x_d) = u^+$. In this case, we would have

$$u^G_j = R(x_j) = \frac{-\theta}{1 - \theta} u_{j+1} + \frac{1}{1 - \theta} u^+. \tag{12}$$

But again considering that the cell fraction θ could be very close to one in practice, we use the linear extrapolation with the conditions that $R(x_{j+2}) = u_{j+2}$ and $R(x_d) = u^+$, giving the following ghost value at the node x_j instead

$$u^G_j = R(x_j) = \frac{-\theta}{2 - \theta} u_{j+2} + \frac{2}{2 - \theta} u^+. \tag{13}$$

As mentioned earlier, to capture the boundary condition across the material interface, we need to keep track of the solution at both sides of the interface as well. Please note that they are also required in calculating the ghost values for points in the neighborhood of the interface. Since the solution of Eq. (1) represents a wave propagating from the left to the right, we calculate u^- by a quadratic extrapolant $Q(x)$ such that $Q(x_{j-2}) = u_{j-2}, Q(x_{j-1}) = u_{j-1}$, and $Q(x_j) = u_j$, i.e.,

$$u^- = Q(x_d) = \frac{\theta(1 + \theta)}{2} u_{j-2} - \theta(2 + \theta) u_{j-1} + \frac{(1 + \theta)(2 + \theta)}{2} u_j, \tag{14}$$

and then calculate u^+ simply by using the jump condition (2), and we have

$$u^+ = \frac{1}{r^+}(g + r^- u^-). \tag{15}$$

3. One-dimensional wave systems

The discretization scheme discussed in Section 2 for scalar wave equations can be extended naturally to the system of one-dimensional linear wave equations

$$\frac{\partial \mathbf{u}}{\partial t} + A \frac{\partial \mathbf{u}}{\partial x} = 0, \quad x \in \Omega = [a, b], \tag{16}$$

where $\mathbf{u}(x,t) = (u_1(x,t), \ldots, u_n(x,t))^{\mathrm{T}}$. The coefficient matrix A has different formulas across the discontinuity $x_d \in (a,b)$ representing a material interface

$$A = \begin{cases} A^-, & x < x_d, \\ A^+, & x > x_d. \end{cases}$$

In general, the solution $\mathbf{u}(x,t)$ will be discontinuous across the interface, and again its values over the left and the right sides of the interface, $\mathbf{u}(x_d^-,t)$ and $\mathbf{u}(x_d^+,t)$, are assumed to be coupled by the given interface jump condition

$$R^+\mathbf{u}(x_d^+,t) - R^-\mathbf{u}(x_d^-,t) = \mathbf{g}(t), \tag{17}$$

where R^+ and R^- are two square matrices.

Again, we seek to develop a uniformly second-order finite difference method based on the Lax–Wendroff approach, which in this case takes the form

$$\mathbf{u}^{n+1} \doteq \mathbf{u}^n + \Delta t \mathbf{u}_t^n + \frac{(\Delta t)^2}{2}\mathbf{u}_{tt}^n = \mathbf{u}^n - \Delta t A \mathbf{u}_x^n + \frac{(\Delta t)^2}{2} A^2 \mathbf{u}_{xx}^n. \tag{18}$$

For each unknown $\mathbf{u}_i^{n+1}$, the above Lax–Wendroff scheme is employed with the spatial derivatives being approximated by second-order central finite differences like in (4) and (5). At such nodes in the neighborhood of the interface, say x_j and x_{j+1}, ghost values $\mathbf{u}_{j+1}^{\mathrm{G}}$ and $\mathbf{u}_j^{\mathrm{G}}$ are defined and used to calculate $\mathbf{u}_j^{n+1}$ and $\mathbf{u}_{j+1}^{n+1}$ in the exactly same fashion as discussed in Section 2 for the case of scalar wave equations.

In general, the coefficient matrix A could have eigenvalues of opposite signs, indicating that waves could propagate through the interface in opposite directions. In this case, quadratic extrapolations similar to (14) are then employed to calculate both $\mathbf{u}^-$ and $\mathbf{u}^+$, the solutions at both sides of the interface. In a hyperbolic problem, however, upwind components of waves should pass through an interface unaffected by downwind contributions. For the numerical solution to satisfy this upwind property as well as the jump condition (17), special treatment has to be introduced.

Suppose that the coefficient matrix A can be diagonalized as

$$A = P\Lambda P^{-1},$$

where $\Lambda = \mathrm{diag}(\lambda_1, \lambda_2, \ldots, \lambda_n)$ in which λ_i's are the eigenvalues of the coefficient matrix A. Without loss of generality, we assume that $\lambda_1, \ldots, \lambda_p > 0$, $\lambda_{p+1}, \ldots, \lambda_q < 0$, and $\lambda_{q+1}, \ldots, \lambda_n = 0$. Also for a well-defined hyperbolic problem, A^- and A^+ are assumed to have the same number of positive eigenvalues as well as the same number of negative ones. Then, by introducing the characteristic variable $\mathbf{w} = (w_1, w_2, \ldots, w_n)^{\mathrm{T}} = P^{-1}\mathbf{u}$, first we can reformulate the jump condition (17) as

$$Q^+\mathbf{w}^+ - Q^-\mathbf{w}^- = \mathbf{g}, \tag{19}$$

where $Q^- = R^-P^-$, $Q^+ = R^+P^+$, and $\mathbf{w}^- = (P^-)^{-1}\mathbf{u}^-$ and $\mathbf{w}^+ = (P^+)^{-1}\mathbf{u}^+$ are the approximations of the characteristic variable $\mathbf{w}$ at the two sides of the discontinuity, respectively. Then we let

$$\mathbf{w}^- = \begin{pmatrix} \mathbf{w}_1^- \\ \mathbf{w}_2^- \\ \mathbf{w}_3^- \end{pmatrix}, \quad \mathbf{w}^+ = \begin{pmatrix} \mathbf{w}_1^+ \\ \mathbf{w}_2^+ \\ \mathbf{w}_3^+ \end{pmatrix}$$

be the partitions of $\mathbf{w}^-$ and $\mathbf{w}^+$ based on the signs of the eigenvalues of the coefficient matrix, i.e., $\mathbf{w}_1 = (w_1, \ldots, w_p)^{\mathrm{T}}$, $\mathbf{w}_2 = (w_{p+1}, \ldots, w_q)^{\mathrm{T}}$, and $\mathbf{w}_3 = (w_{q+1}, \ldots, w_n)^{\mathrm{T}}$, and

$$Q^- = \begin{pmatrix} Q_{11}^- & Q_{12}^- & Q_{13}^- \\ Q_{21}^- & Q_{22}^- & Q_{23}^- \\ Q_{31}^- & Q_{32}^- & Q_{33}^- \end{pmatrix}, \quad Q^+ = \begin{pmatrix} Q_{11}^+ & Q_{12}^+ & Q_{13}^+ \\ Q_{21}^+ & Q_{22}^+ & Q_{23}^+ \\ Q_{31}^+ & Q_{32}^+ & Q_{33}^+ \end{pmatrix} \tag{20}$$

be the corresponding partitions of the matrices Q^- and Q^+, respectively.

The above characteristic components w_1 and w_2 represent, respectively, the characteristic waves propagating along the positive and the negative x direction. Therefore, by the upwind principle, the $\mathbf{w}_1^-$ component of

$\mathbf{w}^-$ and the $\mathbf{w}_2^+$ component of $\mathbf{w}^+$ should not be affected by the embedded boundary, but the $\mathbf{w}_1^+$ component of $\mathbf{w}^+$ and the $\mathbf{w}_2^-$ component of $\mathbf{w}^-$ shall be corrected in an upwind manner. On the other hand, since $\mathbf{w}_3$ represents the non-propagating wave, we can maintain either $\mathbf{w}_3^-$ or $\mathbf{w}_3^+$ while updating characteristic variables by the jump condition (19). In the case that we choose to maintain $\mathbf{w}_3^-$, after rearranging the jump condition (19), we have

$$\begin{pmatrix} Q_{11}^+ & -Q_{12}^- & Q_{13}^+ \\ Q_{21}^+ & -Q_{22}^- & Q_{23}^+ \\ Q_{31}^+ & -Q_{32}^- & Q_{33}^+ \end{pmatrix} \begin{pmatrix} \mathbf{w}_1^+ \\ \mathbf{w}_2^- \\ \mathbf{w}_3^+ \end{pmatrix} = \mathbf{g} + \begin{pmatrix} Q_{11}^- & -Q_{12}^+ & Q_{13}^- \\ Q_{21}^- & -Q_{22}^+ & Q_{23}^- \\ Q_{31}^- & -Q_{32}^+ & Q_{33}^- \end{pmatrix} \begin{pmatrix} \mathbf{w}_1^- \\ \mathbf{w}_2^+ \\ \mathbf{w}_3^- \end{pmatrix}. \tag{21}$$

Here, the coefficient matrix on the left side of Eq. (21) will be invertible for well-posed hyperbolic systems. Once we have the updated characteristic components $\mathbf{w}_1^+$, $\mathbf{w}_2^-$, and $\mathbf{w}_3^+$, the two interface solutions are calculated back by $\mathbf{u}^- = P^-\mathbf{w}^-$ and $\mathbf{u}^+ = P^+\mathbf{w}^+$.

Equivalently, to solve Eq. (16), we can rewrite it as a system of decoupled scalar wave equations

$$\frac{\partial w_i}{\partial t} + \lambda_i \frac{\partial w_i}{\partial x} = 0, \quad 0 \leqslant i \leqslant n, \tag{22}$$

where the λ_i's may have jump discontinuities at the interface. Since each equation in the system (22) is a scalar wave equation, we can solve it by applying the same strategy as discussed in Section 2 trivially. In the case that the transformed jump condition (19) is not decoupled, however, the same procedure to preserve upwind characteristic information and correct downwind one should be carried out to make sure that the numerical approximation satisfies both the upwind property and the jump condition at the interface.

4. Two-dimensional Maxwell's equations

The methodology discussed in Sections 2 and 3 can also be extended naturally to two-dimensional wave problems. For simplicity but without loss of generality, let us consider the two-dimensional z-transverse magnetic (TM) set of Maxwell's equations

$$\frac{\partial \mathbf{u}}{\partial t} + A\frac{\partial \mathbf{u}}{\partial x} + B\frac{\partial \mathbf{u}}{\partial y} = 0, \quad (x,y) \in \Omega = [a,b] \times [c,d], \tag{23}$$

where $\mathbf{u} = (H^x, H^y, E^z)^{\mathrm{T}}$ with E^z and $\mathbf{H} = (H^x, H^y)^{\mathrm{T}}$ representing the scalar electric field and the vector magnetic field, respectively, and

$$A = \begin{pmatrix} 0 & 0 & 0 \\ 0 & 0 & -1/\mu \\ 0 & -1/\varepsilon & 0 \end{pmatrix}, \quad B = \begin{pmatrix} 0 & 0 & 1/\mu \\ 0 & 0 & 0 \\ 1/\varepsilon & 0 & 0 \end{pmatrix}$$

with ε and μ representing the material electric permittivity and the material magnetic permeability, respectively.

In addition, the solution domain Ω is divided by a dielectric interface Γ into two disjoint pieces, Ω^- and Ω^+, representing two distinct dielectric materials. Across the material interface, the tangential components of the fields should be continuous, yielding the following interface condition

$$\mathbf{n} \times \mathbf{H}^+ = \mathbf{n} \times \mathbf{H}^-, \quad \mathbf{n} \cdot \mu^+\mathbf{H}^+ = \mathbf{n} \cdot \mu^-\mathbf{H}^-, \quad E^{z,+} = E^{z,-}, \tag{24}$$

which can be rewritten in a form similar to (17), i.e.,

$$R^+\mathbf{u}^+(\Gamma,t) - R^-\mathbf{u}^-(\Gamma,t) = \mathbf{g}(\Gamma,t), \tag{25}$$

with $\mathbf{g}(\Gamma,t) \equiv 0$ and

$$R^{\pm} = \begin{pmatrix} -n_y & n_x & 0 \\ \mu^{\pm}n_x & \mu^{\pm}n_y & 0 \\ 0 & 0 & 1 \end{pmatrix},$$

where $\mathbf{n} = (n_x, n_y)^{\mathrm{T}}$ represents a unit vector normal to the interface Γ.

To solve Eq. (23) by a finite difference method, the computational domain Ω is discretized into cells of size $\Delta x \times \Delta y$ to form a uniform Cartesian grid $\{(x_i, y_j) = (a + i\Delta x, c + j\Delta y),\ 0 \leqslant i \leqslant N,\ 0 \leqslant j \leqslant M,\ \Delta x = (b-a)/N,\ \Delta y = (d-c)/M\}$. In addition, the intersection points between the interface Γ and the Cartesian grid coordinate lines are also calculated in order to track the solution at both sides of the interface and thus capture the interface condition (25).

As in the one-dimensional case, the upwinding boundary condition capturing method will be constructed again based on the second-order Lax–Wendroff scheme which in the two-dimensional case takes the form

$$\mathbf{u}^{n+1} \doteq \mathbf{u}^n + \Delta t \mathbf{u}_t^n + \frac{(\Delta t)^2}{2}\mathbf{u}_{tt}^n = \mathbf{u}^n - \Delta t(A\mathbf{u}_x^n + B\mathbf{u}_y^n) + \frac{(\Delta t)^2}{2}\left(A^2\mathbf{u}_{xx}^n + (AB+BA)\mathbf{u}_{xy}^n + B^2\mathbf{u}_{yy}^n\right). \tag{26}$$

For each unknown $\mathbf{u}_{ij}^{n+1}$, the above Lax–Wendroff scheme is used together with the spatial derivatives being discretized by central finite differences, yielding the following difference scheme (when $\Delta x = \Delta y$)

$$\begin{aligned}\mathbf{u}_{ij}^{n+1} = \mathbf{u}_{ij}^n - \frac{\Delta t}{2\Delta x}(A(\mathbf{u}_{i+1,j}^n - \mathbf{u}_{i-1,j}^n) + B(\mathbf{u}_{i,j+1}^n - \mathbf{u}_{i,j-1}^n)) + \frac{1}{2}\left(\frac{\Delta t}{\Delta x}\right)^2 (A^2(\mathbf{u}_{i+1,j}^n - 2\mathbf{u}_{ij}^n + \mathbf{u}_{i-1,j}^n) \\ + B^2\left(\mathbf{u}_{i,j+1}^n - 2\mathbf{u}_{ij}^n + \mathbf{u}_{i,j-1}^n\right) + \frac{1}{4}(AB+BA)(\mathbf{u}_{i+1,j+1}^n - \mathbf{u}_{i+1,j-1}^n - \mathbf{u}_{i-1,j+1}^n + \mathbf{u}_{i-1,j-1}^n)).\end{aligned} \tag{27}$$

However, this is valid only at regular grid points, where all nine nodes in the stencil lie on the same side of the interface, and for irregular grid points, local modification of the difference scheme is required for the numerical approximation to maintain the second-order accuracy and preserve the jump condition across the interface.

To construct the local difference scheme for irregular grid points in one side of the interface, ghost values are needed for the correlated irregular grid points at the other side of the interface. The definition of the ghost values, however, becomes more involved for two-dimensional problems. In principle, the calculation of the ghost values for the discretization of spatial derivatives $\mathbf{u}_x$, $\mathbf{u}_{xx}$, $\mathbf{u}_y$, and $\mathbf{u}_{yy}$ could be performed in a dimension by dimension fashion, but this implies that two possibly different ghost values are used at the same ghost node, one value for the numerical discretization in the x direction and the other for that in the y direction. For the numerical discretization of $\mathbf{u}_{xy}$, we then have more than one ghost values to choose for those $(i \pm 1, j \pm 1)$ nodes in the nine point stencil. For example, as shown in Fig. 2, for the numerical discretization of $\mathbf{u}_{xy}$ at the irregular point D, we need a ghost value at the irregular point C that can emulate the behavior of the solution in the subdomain Ω^+. But if we calculate ghost values in a dimension by dimension fashion, there will be two ghost values defined at the node C, one obtained by the linear extrapolation of $\mathbf{u}_{\mathrm{B}}$ and $\mathbf{u}_{\mathrm{II}}^+$, and the other obtained by the linear extrapolation of $\mathbf{u}_{\mathrm{E}}$ and $\mathbf{u}_{\mathrm{III}}^+$.

Another potential problem is that, for an arbitrary interface and an arbitrary grid, the construction of extrapolants (to define ghost values and calculate interface solutions) in the dimension by dimension fashion may not always be possible for some irregular points due to the limited number of neighboring grid points in a specific direction within the same side of the interface. For instance, as shown in Fig. 2, if the interface point II is not too close from the irregular grid point B, we can construct a linear extrapolant of $\mathbf{u}_{\mathrm{B}}$ and $\mathbf{u}_{\mathrm{II}}^+$ to define the corresponding ghost value at the point C in the y direction. When the interface point II is too close to the grid point B, however, as we pointed out in Section 2, we should shift the extrapolation to be centered one grid point to the bottom, i.e., we should use $\mathbf{u}_{\mathrm{A}}$ and $\mathbf{u}^+{}_{\mathrm{II}}$ instead. Unfortunately, the point A is on the other side of the interface and therefore cannot be used here. Although for this particular case, one may argue that we may be able to use $\mathbf{u}_{\mathrm{I}}^+$ and $\mathbf{u}_{\mathrm{II}}^+$ to construct a linear extrapolant in the y direction, it will make programming much more complicated.

Generally speaking, when the interface Γ is flat, there shall be enough grid points for us to construct linear extrapolants to calculate ghost values and interface solutions. For most curved interfaces, however, the dimension by dimension linear extrapolation may not be applicable. For those cases, we propose to use the same least square approach as discussed in [13], using available solutions in one side of the interface, to define a unique ghost value for each irregular point in the other side of the interface. Like in the one-dimensional case, numerical solutions at the interface are also used in the extrapolation for capturing the interface jump condition. Some other general methodology for extrapolating a function from a region where it is known to a region where it is unknown can be found in [31], which is more applicable to moving interface problems though.

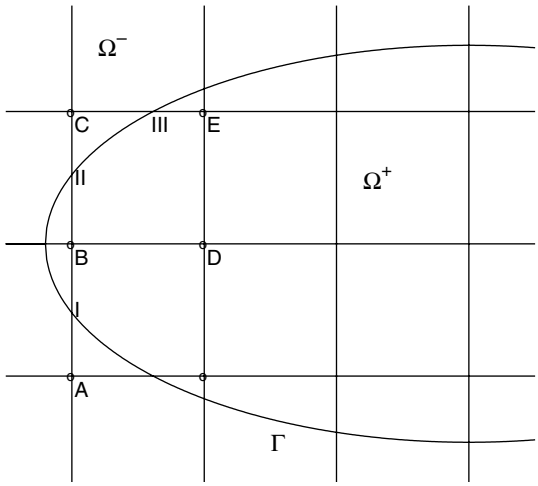

Fig. 2. Illustration of a two-dimensional mesh with an embedded interface Γ.

Once the solutions at all grid points have been calculated, they are used to calculate interface solutions at all interface points by a very similar least square approach. However, like the one-dimensional case, for the numerical solutions to satisfy the interface jump condition (25) and the upwind property, special treatment has to be introduced after the two interface solutions at a particular interface point are obtained by the least square approach.

More precisely, let us consider an interface point $\mathbf{x}_d \in \Gamma$ with the unit normal vector of the embedded boundary at this point being $\mathbf{n} = (n_x, n_y)$. At this point, the system (23) can be projected along the normal direction, yielding the following reformulated linear system

$$\frac{\partial \mathbf{u}}{\partial t} + A_{\mathbf{n}} \frac{\partial \mathbf{u}}{\partial n} + B_\tau \frac{\partial \mathbf{u}}{\partial \tau} = 0, \tag{28}$$

where $\tau = (-n_y, n_x)$ is the unit tangential vector, and $A_{\mathbf{n}} = n_x A + n_y B,\ B_\tau = n_x B - n_y A$.

To use the upwind condition, we need to use the normal and tangential components of the fields with respect to the embedded boundary. Note that the matrix A_{n} has three real eigenvalues c, $-c$ and 0, where $c = 1/(\epsilon\mu)^{1/2}$ is the speed of light in the media, and is thus diagonalizable, i.e.,

$$A_{\mathbf{n}} = P_{\mathbf{n}} \begin{pmatrix} c & & \\ & -c & \\ & & 0 \end{pmatrix} P_{\mathbf{n}}^{-1}.$$

Now, let $\mathbf{u}_d^{-,n+1}$ and $\mathbf{u}_d^{+,n+1}$ be the two interface solutions obtained by a least square approach at $\mathbf{x}_d$. Similar in Section 3, we exploit the characteristic variables corresponding to the normal direction, i.e., $\mathbf{w} = P_{\mathbf{n}}^{-1}\mathbf{u}$. Then in terms of the characteristic variables, the jump condition (25) can be rewritten as

$$Q^+\mathbf{w}^+ - Q^-\mathbf{w}^- = \mathbf{g}, \tag{29}$$

where $Q^- = R^- P_{\mathbf{n}}^-$, $Q^+ = R^+ P_{\mathbf{n}}^+$, and $\mathbf{w}^-$ and $\mathbf{w}^+$ are the approximations of the characteristic variable at $\mathbf{x}_d$, i.e.,

$$\mathbf{w}^- = \begin{pmatrix} w_1^- \\ w_2^- \\ w_3^- \end{pmatrix} = (P_{\mathbf{n}}^-)^{-1}\mathbf{u}_d^{-,n+1}, \quad \mathbf{w}^+ = \begin{pmatrix} w_1^+ \\ w_2^+ \\ w_3^+ \end{pmatrix} = (P_{\mathbf{n}}^+)^{-1}\mathbf{u}_d^{+,n+1}.$$

Note that the characteristic variables w_1 and w_2 represent, respectively, the characteristic waves propagating along $\mathbf{n}$ and $-\mathbf{n}$, and w_3 represents the non-propagating wave. Therefore, by the upwind principle, w_1^- and w_2^+ should not be affected by the embedded boundary since they are upwind incoming with respect to the boundary, while w_1^+ and w_2^- will be affected by the embedded boundary. The non-propagating wave $w_3^\pm$ need not be

corrected across the boundary. Therefore, by letting Q^- and Q^+ be partitioned in a similar way as in (20) based on the signs of the eigenvalues, then w_1^+ and w_2^- can be solved similarly as in (21). Once we have the updated characteristic variables w_1^+ and w_2^-, the two interface solutions are finally calculated by $\mathbf{u}_d^{-,n+1} = P_{\mathbf{n}}^- \mathbf{w}^-$ and $\mathbf{u}_d^{+,n+1} = P_{\mathbf{n}}^+ \mathbf{w}^+$.

As a summary, in the upwinding boundary condition capturing method for Maxwell's equations with general material interfaces, the typical procedures for updating the fields from the time step n to the time step $n+1$ consist of the following steps.

(1) Using the solutions at the time step n in the region $\Omega^{\pm}$, including the interface solutions at the $\pm$ side of the interface, calculate ghost values for all irregular points of the region $\Omega^{\mp}$, $\mathbf{u}_{ij}^{n,\mathrm{G}}$, by extrapolation constructed by a least square approach.
(2) For each regular point (x_i, y_j), apply the standard second-order Lax–Wendroff scheme (27) to find $\mathbf{u}_{ij}^{n+1}$.
(3) For each irregular point (x_i, y_j), use the modified Lax–Wendroff scheme (27) with applicable node values being replaced by corresponding ghost values to calculate $\mathbf{u}_{ij}^{n+1}$.
(4) Using the grid solutions at the time step $n+1$ in the region $\Omega^{\pm}$, calculate the interface solutions at the $\pm$ side of the interface, $\mathbf{u}_d^{\pm,n+1}$, by extrapolation constructed by a least square approach.
(5) At each interface point $\mathbf{x}_d$, correct $\mathbf{u}_d^{\pm,n+1}$ such that they satisfy the interface jump condition as well as the upwind property.

5. Local truncation error and GKS stability analysis

One natural concern with the upwinding boundary condition capturing method is its local truncation error. For the one-dimensional wave Eq. (1), it is well known that the local truncation error for the standard Lax–Wendroff method

$$u_i^{n+1} = \frac{\lambda(\lambda+1)}{2} u_{i-1}^n + (1-\lambda^2) u_i^n + \frac{\lambda(\lambda-1)}{2} u_{i+1}^n, \tag{30}$$

where $\lambda = c\Delta t/\Delta x$, is

$$T_i^n = -\frac{1}{6} c(\Delta x)^2 (1-\lambda^2) u_{xxx}(x_i, t_n) + \mathrm{O}(\Delta t^3).$$

Therefore, at a regular grid point, the upwinding boundary condition capturing method has an $\mathrm{O}(\Delta x^2)$ local truncation error.

To compute the local truncation error at the irregular point x_j, we recall that the solution at this point is given by

$$u_j^{n+1} = \frac{\lambda(\lambda+1)}{2} u_{j-1}^n + (1-\lambda^2) u_j^n + \frac{\lambda(\lambda-1)}{2} u_{j+1}^{n,\mathrm{G}}, \tag{31}$$

where $u_{j+1}^{n,\mathrm{G}}$ is defined by either (8) or (9). As pointed out in Section 2, we use (9) since θ could be very close to zero in practice. Substituting $u_{j+1}^{n,\mathrm{G}}$ defined in (9) into Eq. (31), we have

$$u_j^{n+1} = \frac{\lambda(\lambda+1)}{2} u_{j-1}^n + (1-\lambda^2) u_j^n + \frac{\lambda(\lambda-1)}{2} \left(\frac{\theta-1}{1+\theta} u_{j-1}^n + \frac{2}{1+\theta} u^{-,n} \right). \tag{32}$$

Note that the scheme (32) reduces to the standard Lax–Wendroff scheme when $\theta = 1$. (When $\theta = 0$, it reduces to the upwind method.) Then, it is easy to obtain the local truncation error at x_j

$$T_j^n = \frac{1}{2}(1-\theta) c^- \Delta x (1-\lambda) u_{xx}(x_j, t_n) + \mathrm{O}(\Delta t^2).$$

Similarly, to compute the local truncation error at the irregular point x_{j+1}, we recall that the solution at this point is given by

$$u_{j+1}^{n+1} = \frac{\lambda(\lambda+1)}{2} u_j^{n,\mathrm{G}} + (1-\lambda^2) u_{j+1}^n + \frac{\lambda(\lambda-1)}{2} u_{j+2}^n, \tag{33}$$

where $u_j^{n,\mathrm{G}}$ is defined by either (12) or (13). As pointed out in Section 2, we use (13) since θ could be very close to one in practice. Substituting $u_j^{n,\mathrm{G}}$ defined in (13) into Eq. (33), we have

$$u_{j+1}^{n+1} = \frac{\lambda(\lambda+1)}{2}\left(\frac{-\theta}{2-\theta}u_{j+2}^{n} + \frac{2}{2-\theta}u^{+,n}\right) + (1-\lambda^2)u_{j+1}^{n} + \frac{\lambda(\lambda-1)}{2}u_{j+2}^{n}. \tag{34}$$

Note that the scheme (34) reduces to the standard Lax–Wendroff scheme when $\theta = 0$. (When $\theta = 1$, it reduces to the downwind method but it is not used in the proposed scheme.) Then, it is easy to obtain the local truncation error at x_{j+1}

$$T_{j+1}^{n} = -\frac{1}{2}\theta c^{+}\Delta x(1+\lambda)u_{xx}(x_{j+1}, t_n) + \mathrm{O}(\Delta t^2).$$

Remark 1. It has been theoretically shown and numerically demonstrated that, when a certain order finite difference method is used to approximate mixed initial boundary value problems, the use of a local one-order-lower scheme at a finite number of grid points will not affect the global accuracy of the scheme [4,10,23,32,33]. It is for this reason that we use the linear extrapolations (9) and (13) to define ghost values. As confirmed by numerical experiments in Section 6, the overall second-order convergence rate of the proposed scheme is maintained.

Another natural concern with the upwinding boundary condition capturing method is the stability of the scheme, which is always a critical issue with hyperbolic problems having discontinuous coefficients, and is considerably more complex than for homogeneous cases. For one-dimensional problems it might be possible to analyze this, like that Kreiss et al. did for one-dimensional second-order wave equations with various types of boundary conditions [27–30]. For two-dimensional systems with general curved interfaces, however, there seems to be little hope of proving stability rigorously because of the extensive use of one-sided stencils and one-sided extrapolations in combination with a variable position and shape of the interface.

Next we will analyze the stability of the scheme in the region Ω^{+} using the GKS theory [34–36] for the model wave equation (1) with $c > 0$ and $x_d \leqslant x < \infty$. Recall that the solution $u^{+,n+1}$ is provided through the jump condition (15), the solution u_{j+1}^{n+1} at the point x_{j+1} is given by (34), and the solution u_i^{n+1} for $i > j+1$ is obtained by the standard Lax–Wendroff scheme (30).

For GKS stability analysis, we consider a homogeneous boundary condition at x_d by setting $u^{+,n} = 0$ in (34). Then we have

$$u_{j+1}^{n+1} = (1-\lambda^2)u_{j+1}^{n} + \left(\frac{\lambda(\lambda+1)}{2}\frac{-\theta}{2-\theta} + \frac{\lambda(\lambda-1)}{2}\right)u_{j+2}^{n}. \tag{35}$$

We then need to show that the scheme (30) and (35) does not have any nontrivial admissible solution of the following form

$$u_i^{n} = A(z)z^{n}\kappa^{i}, \qquad |z| \geqslant 1, \qquad |\kappa| \leqslant 1. \tag{36}$$

For the scheme (30) and (35), we have the following system:

$$\begin{aligned} z &= (1-\lambda^2) + \left(\frac{\lambda(\lambda+1)}{2}\frac{-\theta}{2-\theta} + \frac{\lambda(\lambda-1)}{2}\right)\kappa, \\ z &= \frac{\lambda(\lambda+1)}{2}\kappa^{-1} + (1-\lambda^2) + \frac{\lambda(\lambda-1)}{2}\kappa. \end{aligned} \tag{37}$$

Then it is clear that when $\theta = 0$, no solution of any form exists. On the other hand, when $0 < \theta < 1$, it can be seen that

$$\kappa = \sqrt{-\frac{2-\theta}{\theta}}$$

which is greater than 1 in magnitude. Therefore, the system (37) has no admissible solution of the form (36), which proves the GKS stability of the scheme (30) and (35).

6. Numerical examples

To test the second-order accuracy and the stability of the proposed scheme and compare the proposed scheme with the UEBM and the second-order immersed interface method (IIM) [16], several wave systems with available exact solutions, taken from [13], are simulated in this section. As our focus is on the capability of the proposed scheme to handle various types of material interfaces, in all of our numerical examples, the exact solutions are imposed as initial conditions as well as Dirichlet boundary conditions at the boundaries of the computational domains so that we can measure the errors in the numerical solutions and thus investigate the convergence property of the scheme. In practical simulations when exact boundary values are not available, absorbing boundary conditions such as Perfectly Matched Layer (PML) boundary conditions [37–39] should be used. Also, unless otherwise specified, the exact solutions are utilized in defining jump conditions of the type $[\mathbf{u}] = \mathbf{u}^+ - \mathbf{u}^-$ across the material interfaces.

6.1. Linear one-dimensional wave systems

We begin by considering the one-dimensional wave system (16) in the domain $\Omega = [0, 1]$, with the different formulas of the coefficient matrix across the discontinuity $x_d \in (0, 1)$ being

$$A^- = \begin{pmatrix} 0 & 1 \\ 1 & 0 \end{pmatrix} \quad \text{and} \quad A^+ = \begin{pmatrix} 0 & 3 \\ 3 & 0 \end{pmatrix},$$

respectively. Given appropriate initial and boundary conditions, an analytical solution $\mathbf{u} = (u_1, u_2)^{\mathrm{T}}$ to this system is

$$u_1(x,t) = \begin{cases} \frac{1}{2}(\sin(k(x+t)) + \sin(k(x-t))), & 0 \leqslant x < x_d, \\ \frac{1}{2}(\sin(k(x+3t)) + \sin(k(x-3t))), & x_d < x \leqslant 1, \end{cases}$$

and

$$u_2(x,t) = \begin{cases} -\frac{1}{2}(\sin(k(x+t)) - \sin(k(x-t))), & 0 \leqslant x < x_d, \\ -\frac{1}{2}(\sin(k(x+3t)) - \sin(k(x-3t))), & x_d < x \leqslant 1. \end{cases}$$

We shall test four different cases with the discontinuity x_d at $0.5 + \Delta x/10^8, 0.5 + \Delta x/4, 0.5 + \Delta x/2$, and $0.5 - \Delta x/10^8$, corresponding to four different cell fractions $\theta = 10^{-8}$, $1/4$, $1/2$, and $1 - 10^{-8}$, respectively. For all four cases, we set the wave number as $k = 8\pi$ and the time step size as

$$\Delta t = \mathrm{CFL} \times \frac{\Delta x}{|\lambda_{\max}|}, \tag{38}$$

where $|\lambda_{\max}| = \max\{|\lambda_{A^-}|, |\lambda_{A^+}|\}$ and $\mathrm{CFL} = 0.8$ in our tests. Table 1 shows the error analysis results for all four cases, where $\|E\|$ denotes the relative error in the numerical solution measured in L_∞ norm over all grid points at the time $t = 100$ (corresponding to a propagation over a distance of 1200 wavelengths). First, the second-order accuracy of the scheme is clearly observed for all cases. Second, the numerical results also demonstrate the stability of the scheme with the same time step size independent of the interface location. Third,

Table 1
Grid refinement analysis for the one-dimensional wave system

N	$\theta = 10^{-8}$		$\theta = 1/4$		$\theta = 1/2$		$\theta = 1 - 10^{-8}$	
	$\|E\|$	Order	$\|E\|$	Order	$\|E\|$	Order	$\|E\|$	Order
100	1.07E−1		9.72E−2		9.00E−2		9.42E−2	
200	2.30E−2	2.22	2.25E−2	2.11	2.21E−2	2.03	2.29E−2	2.04
400	5.51E−3	2.06	5.45E−3	2.04	5.46E−3	2.02	5.63E−3	2.02
800	1.35E−3	2.02	1.35E−3	2.02	1.36E−3	2.01	1.40E−3	2.01
1600	3.37E−4	2.01	3.35E−4	2.01	3.39E−4	2.00	3.49E−4	2.00

by comparing the numerical results obtained by the proposed scheme to those obtained by the UEBM and the IIM for the same wave system [13], we have found that all three methods have comparable degree of accuracy, which could be partially understood by the fact that all three methods employ the second-order Lax–Wendroff scheme for regular grid points. For instance, if we compare Table 1 to Tables 1–3 in [13], we can see that, in the magnitude of the errors, the proposed approach is slightly better than the UEBM for most cases, in particular, when $N > 100$, but slightly worse than the IIM. However, the implementation of the proposed scheme is more straightforward, especially for multi-dimensional interface problems. Fig. 3 shows the exact and the numerical solutions at the time $t = 100.55$ for the case of $x_d = 0.5 + \Delta x/2$, where the mesh with $N = 200$ is used to calculate the numerical solution. As is indicated, the proposed scheme can correctly capture the interface jump conditions.

6.2. One-dimensional Maxwell's equations

As stated earlier, the standard second-order Yee scheme [1] has been widely used in computational electromagnetics. To compare the proposed method with the standard Yee scheme, we shall consider the one-dimensional Maxwell's equations

$$\epsilon \frac{\partial E}{\partial t} = \frac{\partial H}{\partial z}, \quad \mu \frac{\partial H}{\partial t} = \frac{\partial E}{\partial z},$$

in the domain $\Omega = [-0.5, 0.5]$ or $\Omega = [-0.5, 0.51]$, where $E(z,t)$ and $H(z,t)$ signify the mutually perpendicular tangential electric and magnetic field components E_y and H_x, respectively.

We take the simple example of a plane wave normally incident on a planar boundary ($z = 0$). On the left of the boundary ($z \leqslant 0$), the medium is vacuum ($\epsilon_1 = 1,\ \mu_1 = 1$), but on the right ($0 \leqslant z$), the medium is a dielectric with $\epsilon_2 = 2$ and $\mu_2 = 2$. When the incident wave encounters the interface between the vacuum and the dielectric, a reflective wave and a transmitted wave will be generated, respectively. To solve the wave propagation problem, the above one-dimensional Maxwell's equations are employed. In our test, the incident plane wave takes the form

$$E_{\text{inc}} = \mathrm{e}^{\mathrm{i}(\omega t + k_1 z)}, \quad H_{\text{inc}} = \frac{1}{Z_1}\mathrm{e}^{\mathrm{i}(\omega t + k_1 z)},$$

where $k_1 = \omega(\epsilon_1\mu_1)^{1/2}$ and $Z_1 = (\mu_1/\epsilon_1)^{1/2}$ are the propagation constant and the impedance of the vacuum, respectively. An analytical solution to this problem is given in [13,40].

We first solve the above one-dimensional Maxwell's equations in the domain $\Omega = [-0.5, 0.5]$ by the Yee scheme and the proposed scheme with CFL = 0.8. Note that the computational domain for this case is

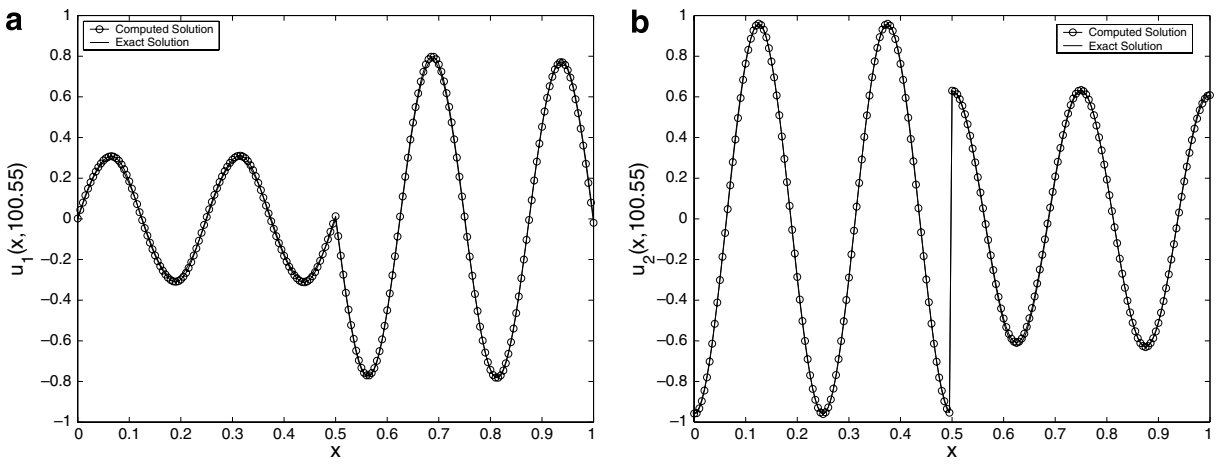

Fig. 3. The exact and the numerical solutions of the one-dimensional wave system at the time $t = 100.55$ for the case of $x_d = 0.5 + \Delta x/2$, where the mesh with $N = 200$ is used to calculate the numerical solution. (a) $u_1(x, 100.55)$. (b) $u_2(x, 100.55)$.

Table 2
Grid refinement analysis for the one-dimensional Maxwell's equations with $\Omega = [-0.5, 0.5]$

N	The Yee scheme		The proposed scheme	
	$\|E\|$	Order	$\|E\|$	Order
100	2.41E−1		1.46E−2	
200	6.12E−2	1.98	3.65E−3	2.00
400	1.53E−2	2.00	9.11E−4	2.00
800	3.83E−3	2.00	2.28E−4	2.00
1600	9.59E−4	2.00	5.70E−5	2.00

symmetric about the interface. So for the chosen grid sizes, the interface is always on a grid point, i.e., $\theta = 0$ for the proposed scheme. For the Yee scheme, we thus always place the dielectric interface on a magnetic node for the chosen grid sizes, and the permeability μ at this magnetic node is simply taken as the arithmetic average of μ_1 and μ_2. Table 2 shows the results of grid refinement analysis for both schemes, where the relative error $\|E\|$ is measured at the time $t = 100$, clearly indicating the expected second-order convergence rate for both the Yee scheme and the proposed scheme. In addition, for this problem the UEBM seems to be a little better than the proposed approach in the magnitude of the errors as shown in Table 2 in this paper and Table 5 in [13].

We then solve the above one-dimensional Maxwell's equations in a slightly different domain $\Omega = [-0.5, 0.51]$ by the Yee scheme and the proposed scheme with the same CFL number. Note that the computational domain for this case is not symmetric about the interface. So for the chosen grid sizes, the interface is not necessarily on a grid point, and for the proposed scheme, the cell fraction θ varies between around 0.01 and 0.51. For the Yee scheme, the same code as in the case of $\Omega = [-0.5, 0.5]$ is used, but now we can no longer guarantee the interface to be placed on an either magnetic or electric node for the chosen grid sizes. The relative errors $\|E\|$ measured at the same time $t = 100$ are displayed in Table 3.

As shown in Table 3, the numerical solution obtained by the proposed scheme maintains the second-order convergence rate, but that obtained by the standard Yee scheme seems to be only first-order accurate at best, even though for this case the solution is continuous across the interface. Furthermore, the convergence rate of the Yee scheme tends to decrease as the grid size increases, which could be partially understood by the possible localized non-convergent behavior of the scheme, as reported by many authors [3,4]. Another point that can be appreciated from the numerical results is that, to have numerical solutions of a realistic accuracy around 1%, the grid size N needed by the Yee scheme is about a factor of 4 larger than that needed by the proposed scheme. Therefore, in terms of the grid size, the proposed scheme is practically more efficient than the standard Yee scheme for modeling dielectric interfaces.

6.3. Linear two-dimensional wave systems

To verify the second-order accuracy of the proposed scheme for two-dimensional applications, we start by considering a two-dimensional wave system (23) with the two coefficient matrices in the domain Ω^- being

$$A^- = \begin{pmatrix} 2 & -1 \\ -1 & 2 \end{pmatrix}, \quad B^- = \begin{pmatrix} 2 & 0 \\ 0 & 1 \end{pmatrix},$$

Table 3
Grid refinement analysis for the one-dimensional Maxwell's equations with $\Omega = [-0.5, 0.51]$

N	The Yee scheme		The proposed scheme		
	$\|E\|$	Order	$\|E\|$	Order	θ
100	5.50E−2		1.53E−2		0.5050
200	3.00E−2	0.88	3.83E−3	2.00	0.0099
400	1.34E−2	1.16	9.46E−4	2.02	0.0198
800	7.69E−3	0.81	2.35E−4	2.01	0.0396
1600	5.30E−3	0.54	5.84E−5	2.01	0.0792

and in the domain Ω^+ being

$$A^+ = \begin{pmatrix} 4 & -2 \\ -2 & 4 \end{pmatrix}, \quad B^+ = \begin{pmatrix} 4 & 0 \\ 0 & 2 \end{pmatrix},$$

respectively. Given appropriate initial and boundary conditions, an analytical solution to this system is

$$u_1(x,y,t) = \begin{cases} \sin(k(x-t)) + \sin(k(y-2t)), & (x,y) \in \Omega^-, \\ \sin(k(x-2t)) + \cos(k(y-4t)), & (x,y) \in \Omega^+, \end{cases}$$

and

$$u_2(x,y,t) = \begin{cases} \sin(k(x-t)) + \sin(k(y-t)), & (x,y) \in \Omega^-, \\ \sin(k(x-2t)) + \cos(k(y-2t)), & (x,y) \in \Omega^+. \end{cases}$$

For the purpose of testing the capability of the proposed scheme in handling different types of material interfaces, we shall solve the above two-dimensional wave system in the square domain $\Omega = [-1,1] \times [-1,1]$ with several types of interfaces. For all cases, however, the wave number is set as $k = 2\pi$ and the time step size as

$$\Delta t = \mathrm{CFL} \times \frac{h}{2\sqrt{2}\ |\lambda_{\max}|}, \tag{39}$$

where $|\lambda_{\max}| = \max\{|\lambda_{A^-}|, |\lambda_{A^+}|, |\lambda_{B^-}|, |\lambda_{B^+}|\}$, $h = \Delta x = \Delta y$, and in our tests CFL = 0.8, independent of the location and the shape of the interface.

We first consider the case in which the interface Γ is a straight line represented by the equation $y = x + h_\Gamma$, where $0 < h_\Gamma < \Delta x$ signifies the distance between the interface Γ and the grid points. A small h_Γ implies that the interface is close to the grid points from above, and on the other hand, a large h_Γ indicates that the interface is close to the grid points from below. Ω^- and Ω^+ are the regions described by $y > x + h_\Gamma$ and $y < x + h_\Gamma$, respectively. Note that in this case, ghost values are also required for some boundary points in the bottom-left and the upper-right corners of the square. In Table 4, we list the errors in the numerical solution measured at the time $t = 100$ and the corresponding error analysis results for three different situations with h_Γ being chosen as $10^{-8}\Delta x$, $\Delta x/2$, and $(1\text{–}10^{-8})\Delta x$, respectively. Again, a uniformly second-order convergence is observed in all three situations. Also, by comparing Table 4 in this paper to Table 6 in [13], we can see that the proposed approach clearly outperforms the UEBM with around twice the accuracy. Fig. 4 shows the numerical solution of $u_1(x,y,t)$ at the time $t = 100$ for the case of $h_\Gamma = 10^{-8}\Delta x$ with a 200×200 grid. As can be seen, the numerical solution properly captures the interface jump condition.

We then consider the two-dimensional wave system with a non-ideal circular interface Γ defined by $x^2 + y^2 = (1 + \Delta r \sin L\phi)^2 0.6^2$, where Δr represents a variation of the radius of the non-ideal circular interface, L the number of the deviation maxima, and ϕ the polar angle of the point (x,y). Here, the interface is a superposition of random Gaussian deviation from an ideal circular interface of radius $R = 0.6$ with a maximal amplitude Δr and a characteristic distance between the deviation maxima $\Delta l \approx 2\pi R/L$. Ω^- and Ω^+ are the regions outside and inside the circular interface, respectively. Note that in this case, depending on the location of an interface point, the two eigenvalues of the matrix $A_n = n_x A + n_y B$ could be both positive, both negative, or one positive and one negative. The errors in the numerical solution measured at the time $t = 100$ are shown in Table 5, which again confirms the second-order convergence rate of the proposed scheme. Moreover, by comparing Table 5 in this paper to Table 8 in [13], we can see once again that the proposed approach clearly

Table 4
Grid refinement analysis for the two-dimensional wave system with the straight line interface: $y = x + h_\Gamma$

Grid	$h_\Gamma = 10^{-8}\Delta x$		$h_\Gamma = \Delta x/2$		$h_\Gamma = (1 - 10^{-8})\Delta x$	
	$\|E\|$	Order	$\|E\|$	Order	$\|E\|$	Order
100×100	4.30E−2		4.36E−2		4.93E−2	
200×200	1.08E−2	1.99	1.08E−2	2.02	1.09E−2	2.18
400×400	2.71E−3	1.99	2.70E−3	2.00	2.74E−3	2.00
800×800	6.78E−4	2.00	6.77E−4	2.00	6.77E−4	2.01

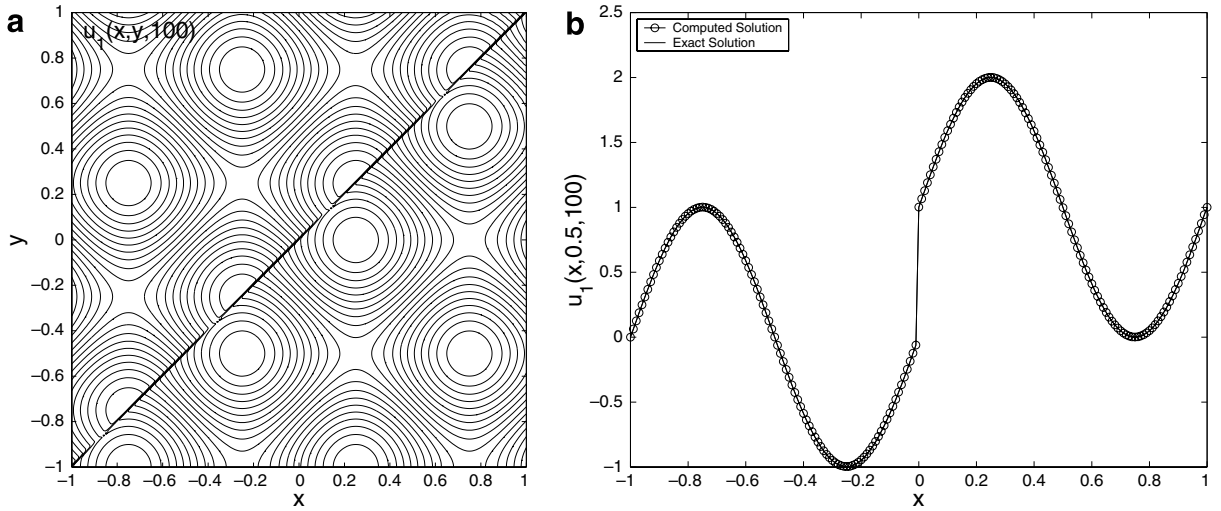

Fig. 4. The exact and the numerical solutions $u_1(x, y, t)$ of the two-dimensional wave system at the time $t = 100$ for the case of the straight line interface $y = x + 10^{-8}\Delta x$, where a 200×200 grid is used to calculate the numerical solution. (a) The contour of the numerical solution. (b) The $y = 0.5$ cross-sections of the numerical and the exact solutions.

Table 5
Grid refinement analysis for the two-dimensional wave system with the non-ideal circular interface: $x^2 + y^2 = (1 + \Delta r \sin L\phi)^2 0.6^2$

Grid	$\Delta r = 0.0$		$L = 10,\ \Delta r = 0.05$		$L = 20,\ \Delta r = 0.025$	
	$\|E\|$	Order	$\|E\|$	Order	$\|E\|$	Order
100×100	3.73E−2		3.74E−2		3.46E−2	
200×200	6.31E−3	2.56	6.60E−3	2.50	6.48E−3	2.42
400×400	1.57E−3	2.01	1.54E−3	2.10	1.56E−3	2.05
800×800	3.94E−4	2.00	3.91E−4	1.98	3.95E−4	1.99

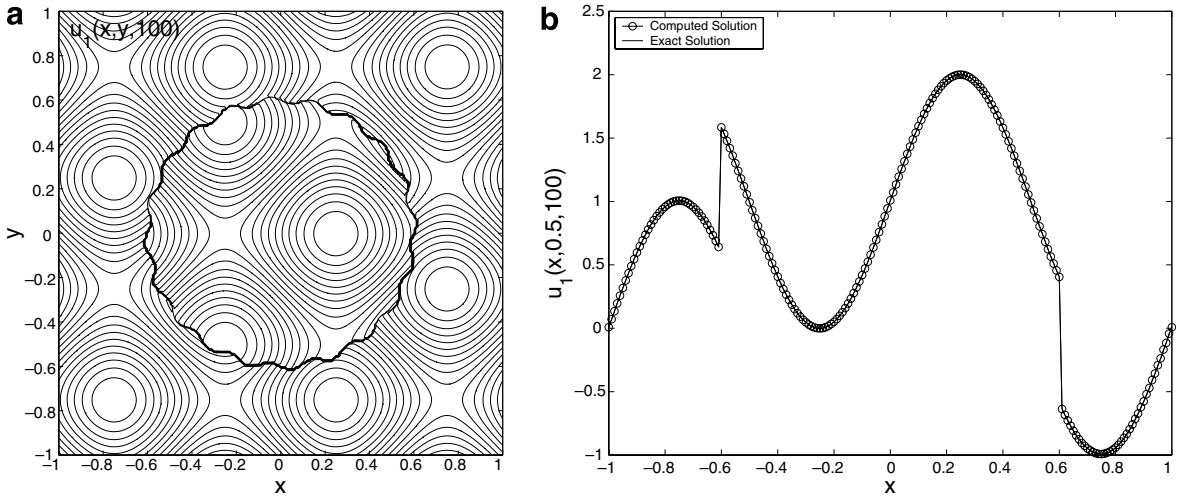

Fig. 5. The exact and the numerical solutions $u_1(x, y, t)$ of the two-dimensional wave system at the time $t = 100$ for the case of the non-ideal circular interface $x^2 + y^2 = (1 + 0.025 \sin 20\phi)^2 0.6^2$, where a 200×200 grid is used to calculate the numerical solution. (a) The contour of the numerical solution. (b) The $y = 0.5$ cross-sections of the numerical and the exact solutions.

outperforms the UEBM with around twice the accuracy. The contour as well as the $y = 0.5$ cross-section of the numerical solution of $u_1(x, y, t)$ at the same time are plotted in Fig. 5, which again demonstrates the capability of the proposed scheme in capturing discontinuity of the solution at the interfaces.

We next consider the same two-dimensional wave system with a multiple bubble interface Γ that consists of four circles defined by $(x+0.5)^2 + y^2 = 0.3^2$, $(x-0.6)^2 + y^2 = 0.25^2$, $x^2 + (y+0.6)^2 = 0.25^2$ and $x^2 + (y-0.6)^2 = 0.25^2$, respectively. And for this example, we let the region outside the four circles be Ω^+ and the region enclosed by the four circles be Ω^-. The errors in the numerical solution measured at the time $t = 100$ are shown in Table 6, and the contour as well as the $y = 0.5$ cross-section of the numerical solution of $u_1(x, y, t)$ at the same time is plotted in Fig. 6, which again demonstrate the scheme's second-order convergence and its capability in capturing discontinuity of the solution at the interface.

To examine the long time stability of our approach, we record and display in Fig. 7 the corresponding errors of the numerical solution as a function of time over the time period $[0, 100]$ for various grid sizes for both the straight line interface and the non-ideal circular interface (A total of 848,520 time steps are carried out for the 800×800 grid). Note that there is no noticeable growth of the error after running the problem for 100 time units, indicating the scheme will remain stable and second-order accurate for long time computations.

6.4. Scattering by single dielectric cylinder

In this example, we shall consider a typical electromagnetic scattering problem as illustrated in Fig. 8, i.e., scattering of a plane incident wave by a dielectric circular cylinder. Maxwell's equations (23), together with the boundary condition (24), can be used to solve the problem.

Table 6
Grid refinement analysis for the two-dimensional wave system with the multiple bubble interface

Grid	$\|E\|$	Order	Time steps
200×200	9.26E−3		212,130
400×400	2.32E−3	2.00	424,260
800×800	5.86E−4	1.99	848,520

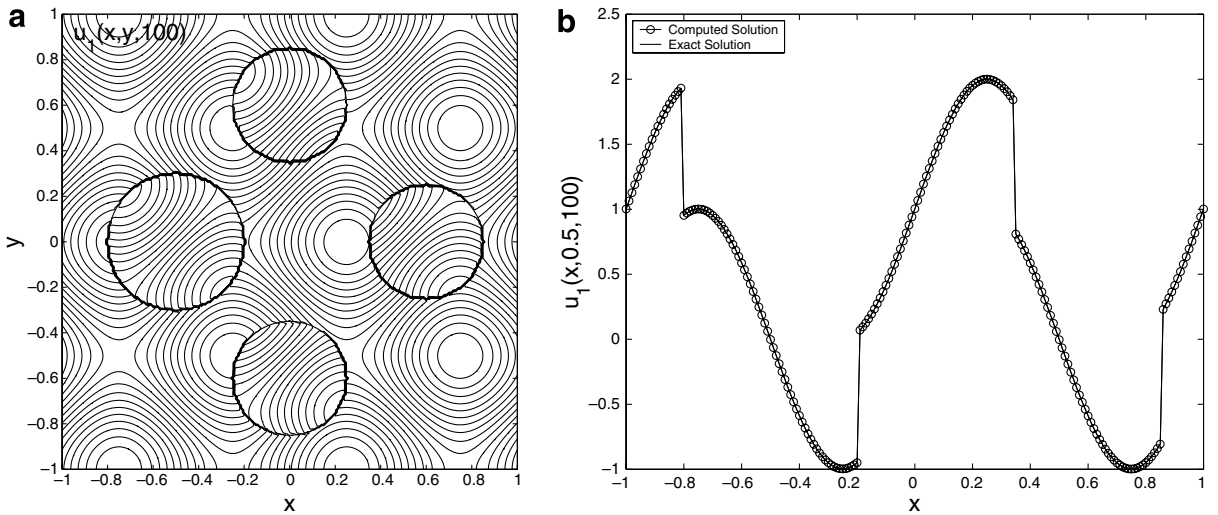

Fig. 6. The exact and the numerical solutions $u_1(x, y, t)$ of the two-dimensional wave system at the time $t = 100$ for the case of the multiple bubble interface, where a 200×200 grid is used to calculate the numerical solution. (a) The contour of the numerical solution. (b) The $y = 0.5$ cross-sections of the numerical and the exact solutions.

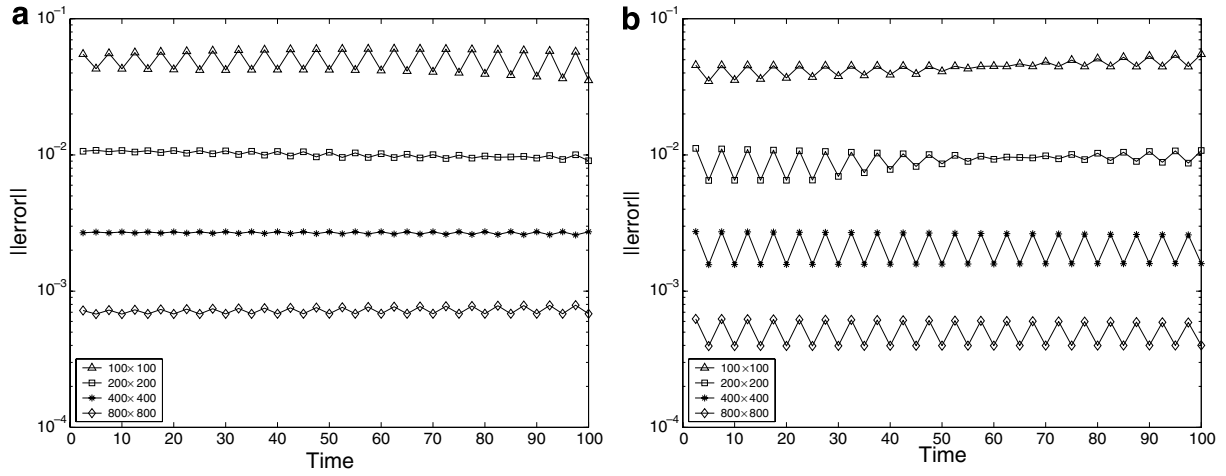

Fig. 7. The L_∞ error in the numerical solution as a function of time for the two-dimensional wave system over the time period $[0, 100]$ for different grid sizes. (a) The straight line interface: $y = x + 10^{-8}\Delta x$. (b) The non-ideal circular interface: $x^2 + y^2 = (1 + 0.025\sin 20\phi)^2 0.6^2$.

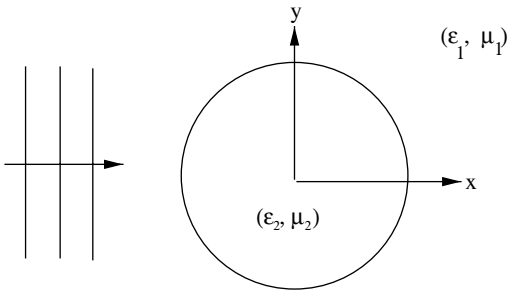

Fig. 8. Illustration of scattering of a plane incident wave by a dielectric circular cylinder.

We assume that the cylinder is illuminated by a time-harmonic incident plane wave of the form

$$E^z_{\text{inc}} = \mathrm{e}^{-\mathrm{i}(k_1 x - \omega t)}, \quad H^y_{\text{inc}} = -\mathrm{e}^{-\mathrm{i}(k_1 x - \omega t)},$$

where $k_1 = \omega(\mu_1\epsilon_1)^{1/2}$ is the propagation constant for homogeneous, isotropic free space medium. Then there is an analytical solution of this problem due to Mie, which can be found in [41] and is also available in [13].

We would like to verify the second-order convergence of the proposed scheme for solving the above practical scattering problem. To this end, the analytical solution of the problem is imposed as the initial condition as well as the Dirichlet boundary condition at the artificial boundary of the computational domain. Also, in our simulations we let the cylinder radius R be 0.5 and the angular frequency Ω of the incident wave be 2π. The computational domain is the square $\Omega = [-1, 1] \times [-1, 1]$, and the time step size is always imposed as

$$\Delta t = \mathrm{CFL} \times \frac{h}{2\sqrt{2}\lambda_{\max}},$$

where $\lambda_{\max} = \max\{c_1, c_2\}$ and $c_k = 1/(\varepsilon_k\mu_k)^{1/2}$, for $k = 1, 2$, and $\mathrm{CFL} = 0.8$ in our tests. Please note that $\lambda_{\max} = 1$ in our case since the material exterior to the cylinder is assumed to be vacuum ($\varepsilon_1 = 1$ and $\mu_1 = 1$).

We first consider a situation in which $\varepsilon_2 = 2$ but $\mu_2 = 1$, i.e., the material is non-magnetics. Fig. 9 shows the contour and the $x = 0.2$ cross-section of the computed field component H^x at the time $t = 10$ when using a 200×200 mesh. Please note that H^x is continuous but its derivative is discontinuous across the material interface. Actually, in this case, it is clear from the interface condition (24) that all three field components are continuous across the material interface. The derivative of the E^z component is also continuous across the interface, but the derivatives of the H^x and H^y components are discontinuous.

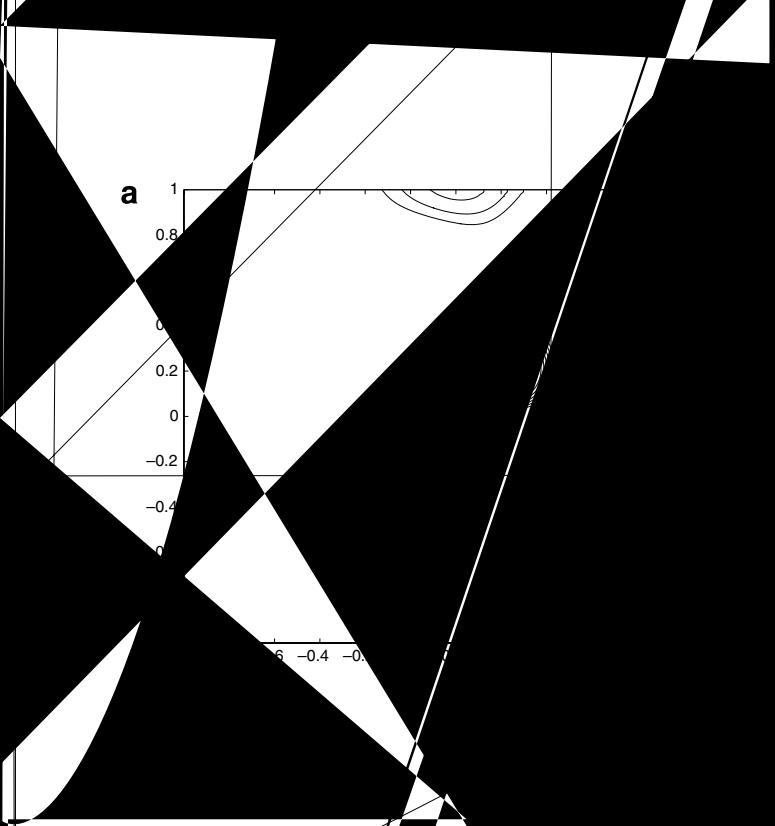

We then consider a cas[illegible] whic[illegible] of the computed field co[illegible]onent H[illegible] case, both H^x and its de[illegible]ative are di[illegible] the interface condition[illegible]) that in thi[illegible] nents H^x and H^y an[illegible]e derivatives o[illegible] interface.

Table 7 shows th[illegible]ror analysis results fo[illegible] solution measured [illegible]L_∞ norm over all grid p[illegible] grid size, first the [illegible]bal second-order accurac[illegible] for the first case is [illegible]tter than that for the second case, whic[illegible]

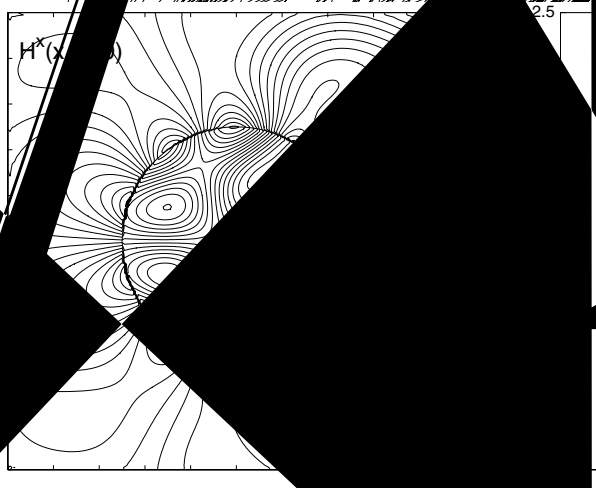

Table 7
Grid refinement analysis for solving the scattering problem by the proposed scheme ($\varepsilon_1 = 1,\ \varepsilon_2 = 2,\ \mu_1 = 1,\ \mu_2 = 1$ or 2)

Grid	$\mu_2 = 1$		$\mu_2 = 2$	
	$\|E\|$	Order	$\|E\|$	Order
100×100	4.87E−2		1.83E−1	
200×200	1.28E−2	1.92	4.07E−2	2.17
400×400	3.29E−3	1.96	9.67E−3	2.07
800×800	8.22E−4	2.00	2.44E−3	1.98

Table 8
Grid refinement analysis for solving the scattering problem by the standard Yee scheme ($\varepsilon_1 = 1,\ \varepsilon_2 = 2,\ \mu_1 = 1,\ \mu_2 = 1$ or 2)

Grid	$\mu_2 = 1$		$\mu_2 = 2$	
	$\|E\|$	Order	$\|E\|$	Order
100×100	2.65E−2		8.31E−2	
200×200	1.26E−2	1.07	1.05E−1	
400×400	6.26E−3	1.01	1.17E−1	
800×800	3.32E−3	0.91	1.18E−1	

the second case is a factor of $\sqrt{2}$ smaller than that for the first case and thus a smaller grid size shall be needed to resolve the solution to the same degree of accuracy.

As our final numerical example, we would like to investigate the efficiency of the proposed method by comparing it against the standard Yee scheme in solving the same scattering problems. The errors in the numerical solutions for the Yee scheme are displayed in Table 8. As indicated, for the case that $\mu_2 = 1$ (the solutions are continuous), the Yee scheme converges, but the global accuracy of the Yee scheme is reduced to first-order because it cannot model the interface correctly. On the other hand, for the case that $\mu_2 = 2$ (the solutions are discontinuous), the standard Yee scheme once again exhibits the non-convergent behavior.

7. Conclusions

In this paper, with the use of ghost points, we have proposed a second-order upwinding boundary condition capturing method for solving time-domain Maxwell's equations in media with material interfaces. The proposed scheme retains the simplicity of Cartesian grid based methods while providing the uniformly second-order accuracy across the material interfaces at a time step size allowed on the uniform Cartesian mesh. Extensive numerical tests confirm the stability and the global second-order accuracy and ease of implementation of the method. In addition, although the proposed scheme in general has comparable degree of accuracy with previous embedded boundary methods including the second-order UEBM and the second-order IIM, the proposed approach outperforms the UEBM for most cases, in particular, when used to solve two-dimensional wave systems.

Acknowledgments

This work was supported, in part, by funds provided by the University of North Carolina at Charlotte.

References

[1] K.S. Yee, Numerical solution of initial boundary value problems involving Maxwell equations in isotropic media, IEEE Trans. Antennas Propagat. 14 (3) (1966) 302–307.
[2] A. Taflove, S.C. Hagness, Computational Electrodynamics: The Finite-Difference Time-Domain Method, third ed., Artech House, Boston, 2005.
[3] P. Monk, E. Suli, Error estimates of Yee's method on nonuniform grids, IEEE Trans. Magn. 30 (5) (1994) 3200–3203.

[4] A. Ditkowski, K. Dridi, J.S. Hesthaven, Convergent Cartesian grid methods for Maxwell's equations in complex geometries, J. Comput. Phys. 170 (5) (2001) 39–80.
[5] A. Ditkowski, J.S. Hesthaven, C.H. Teng, Modeling dielectric interfaces in the FDTD-method: a comparative study, in: 2000 Progress in Electromagnetics Research (PIERS 2000) Proceedings, Cambridge, MA, July 5–14, 2000.
[6] T. Xiao, Q.H. Liu, A staggered upwind embedded boundary method to eliminate the FDTD staircasing error, IEEE Trans. Antennas Propagat. 52 (3) (2004) 730–741.
[7] J.S. Hesthaven, High-order accurate methods in time-domain computational electromagnetics. A review, Adv. Imag. Electron Phys. 127 (2003) 59–117.
[8] A. Yefet, P.G. Petropoulos, A staggered fourth order accurate explicit finite difference scheme for the time-domain Maxwell's equations, J. Comput. Phys. 168 (2) (2001) 286–315.
[9] A. Yefet, E. Turkel, Fourth order compact implicit method for the Maxwell equations with discontinuous coefficients, Appl. Numer. Math. 33 (1) (2000) 125–134.
[10] Z.Q. Xie, C.H. Chan, B. Zhang, An explicit fourth order staggered finite-difference time-domain method for Maxwell's equations, J. Comput. Appl. Math. 147 (1) (2002) 75–98.
[11] Z.Q. Xie, C.H. Chan, B. Zhang, An explicit fourth order orthogonal curvilinear staggered-grid FDTD method for Maxwell's equations, J. Comput. Phys. 175 (2) (2002) 739–763.
[12] S. Zhao, G.W. Wei, High-order FDTD methods via derivative matching for Maxwell's equations with material interfaces, J. Comput. Phys. 200 (1) (2004) 60–103.
[13] W. Cai, S. Deng, An upwinding embedded boundary method for Maxwell's equations in media with material interfaces: 2D case, J. Comput. Phys. 190 (1) (2003) 159–183.
[14] M.J. Berger, C. Helzel, R.J. LeVeque, *h*-box methods for the approximation of hyperbolic conservation laws on irregular grids, SIAM J. Numer. Anal. 41 (3) (2003) 893–918.
[15] J.B. Bell, P. Collella, W.Y. Crutchfield, M. Welcome, An adaptive Cartesian grid method for unsteady compressible flow in irregular regions, J. Comput. Phys. 120 (2) (1995) 278–304.
[16] C. Zhang, R.J. LeVeque, The immersed interface method for acoustic wave equations with discontinuous coefficients, Wave Motion 25 (3) (1997) 237–263.
[17] R. Fedkiw, T. Aslam, B. Merriman, S. Osher, A non-oscillatory Eulerian approach to interfaces in multimaterial flows (the ghost fluid method), J. Comput. Phys. 152 (2) (1999) 457–492.
[18] R. Fedkiw, T. Aslam, S. Xu, The ghost fluid method for deflagration and detonation discontinuities, J. Comput. Phys. 154 (2) (1999) 393–427.
[19] X.D. Liu, R. Fedkiw, M. Kang, A boundary condition capturing method for Poisson's equation on irregular domains, J. Comput. Phys. 160 (1) (2000) 151–178.
[20] M. Kang, R. Fedkiw, X.D. Liu, A boundary condition capturing method for multiphase incompressible flow, J. Sci. Comput. 15 (3) (2000) 323–360.
[21] D. Nguyen, R. Fedkiw, M. Kang, A boundary condition capturing method for incompressible flame discontinuities, J. Comput. Phys. 172 (1) (2001) 71–98.
[22] F. Gibou, R. Fedkiw, L.T. Cheng, M. Kang, A second-order-accurate symmetric discretization of the Poisson equation on irregular domains, J. Comput. Phys. 176 (1) (2002) 205–227.
[23] F. Gibou, R. Fedkiw, A fourth order accurate discretization for the Laplace and heat equations on arbitrary domains, with applications to the Stefan problem, J. Comput. Phys. 202 (2) (2005) 577–601.
[24] X.Y. Hu, B.C. Khoo, An interface interaction method for compressible multifluids, J. Comput. Phys. 198 (1) (2004) 35–64.
[25] B. Lombard, J. Piraux, Numerical treatment of two-dimensional interfaces for acoustic and elastic waves, J. Comput. Phys. 195 (1) (2004) 90–116.
[26] K. Yokoia, F. Xiao, H. Liu, K. Fukasaku, Three-dimensional numerical simulation of flows with complex geometries in a regular Cartesian grid and its application to blood flow in cerebral artery with multiple aneurysms, J. Comput. Phys. 202 (1) (2005) 1–19.
[27] H.O. Kreiss, N.A. Petersson, J. Yström, Difference approximations for the second order wave equation, SIAM J. Numer. Anal. 40 (5) (2002) 1940–1967.
[28] H.O. Kreiss, N.A. Petersson, A second order accurate embedded boundary method for the wave equation with Dirichlet data, SIAM J. Sci. Comput. 27 (4) (2006) 1141–1167.
[29] H.O. Kreiss, N.A. Petersson, J. Yström, Difference approximations of the Neumann problem for the second order wave equation, SIAM J. Numer. Anal. 42 (2) (2004) 1292–1323.
[30] H.O. Kreiss, N.A. Petersson, An embedded boundary method for the wave equation with discontinuous coefficients, UCRL-JRNL 215702, Lawrence Livermore National Lab, 2005.
[31] T. Aslam, A partial differential equation approach to multidimensional extrapolation, J. Comput. Phys. 193 (1) (2003) 349–355.
[32] G. Gustafsson, The convergence rate for difference approximations to mixed initial boundary value problems, Math. Comput. 29 (1975) 396–406.
[33] G. Gustafsson, The convergence rate for difference approximations to general mixed initial boundary value problems, SIAM J. Numer. Anal. 18 (2) (1981) 179–190.
[34] H.O. Kreiss, Stability theory for difference approximations of mixed initial boundary value problems I, Math. Comput. 22 (1968) 703–714.
[35] B. Gustafsson, H.O. Kreiss, A. Sundstrom, Stability theory of difference approximations for mixed initial boundary value problems II, Math. Comput. 26 (1972) 649–686.

[36] J. Strikewerda, Finite Difference Schemes and Partial Differential Equations, Wadsworth and Brooks/Cole, 1989.
[37] J.P. Berenger, A perfectly matched layer for the absorption of electromagnetic waves, J. Comput. Phys. 114 (2) (1994) 185–200.
[38] R. Ziolkowski, Time derivative Lorentz model based absorbing boundary condition, IEEE Trans. Antennas Propagat. 45 (10) (1997) 1530–1535.
[39] S. Abarbanel, D. Gottlieb, On the construction and analysis of absorbing layers in CEM, Appl. Numer. Math. 27 (4) (1998) 331–340.
[40] P. Lorrain, D. Corson, F. Lorrain, Electromagnetics Fields and Waves, Freeman, New York, 1988.
[41] K. Umashankar, A. Taflove, Computational Electrodynamics, Artech House, Boston, 1993.